scientific data

Check for updates

OPEN

DATA DESCRIPTOR

Comprehensive multi-phase 3D contrast-enhanced CT imaging for primary liver cancer

Jiawei Luo[1], Xiaoyu Wan[2], Jinchao Du[3], Li Liu[4], Ling Zhao[4], Xin Peng[4], Min Wu[5], Shixin Huang[6] ✉ & Xixi Nie[7] ✉

Primary liver cancer is a significant global health issue with high incidence and mortality rates worldwide. Accurate diagnosis and classification of its subtypes are crucial for choosing the right treatment options and improving patient outcomes. Contrast-enhanced computed tomography (CECT) is known for its high sensitivity and specificity in diagnosing liver cancer. However, publicly available datasets of liver cancer CECT scans are limited and often do not fully cover all subtypes or include complete CT scan phases. We hypothesize that using 3D CECT images with complete scan phases can help develop and validate diagnostic and segmentation models for primary liver cancer. Therefore, we created a CECT dataset with annotated liver and lesion areas. This dataset includes 278 cases of liver cancer, featuring hepatocellular carcinoma, intrahepatic cholangiocarcinoma, and combined hepatocellular-cholangiocarcinoma, along with CECT images from 83 non-liver cancer subjects. It contains over 50,000 layers of liver cancer lesion images. We believe this dataset can offer valuable support for developing and validating models for classifying and segmenting primary liver cancer.

Background and Summary

Primary liver cancer ranks as the sixth most common cancer worldwide, with approximately 905,677 new cases annually and causing about 830,180 deaths each year, making it the third leading cause of cancer-related mortality globally[1,2]. Effective early detection and accurate diagnosis are paramount, as they significantly enhance the likelihood of successful treatment outcomes and survival rates[3]. Furthermore, precise diagnostic processes are critical in selecting optimal treatment strategies, which can help minimize recurrence and improve patients' overall quality of life. Primary liver cancer comprises several subtypes, including Hepatocellular Carcinoma (HCC), Intrahepatic Cholangiocarcinoma (ICC), and Combined Hepatocellular-Cholangiocarcinoma (cHCC-CCA), each requiring tailored treatment approaches[4–6]. Therefore, accurate and early diagnosis is essential for effective treatment planning and improved prognoses[7].

Contrast-enhanced computed tomography (CECT) is a valuable tool in the detection and characterization of liver cancer[8,9]. It offers high sensitivity and specificity, particularly in identifying hypervascular tumors like HCC, which show strong enhancement in the arterial phase. CECT also helps assess tumor vascularity, important for determining tumor aggressiveness and planning treatments[10,11]. Radiologists and oncologists often use CECT to examine abnormalities in the liver's structure and texture, which are crucial markers for diagnosing and monitoring primary liver tumors. A liver CECT scan typically includes four key phases: the Plain (Non-Contrast) Phase, Arterial Phase, Venous Phase, and Delayed Phase. These imaging phases are crucial for a thorough evaluation of the vascular characteristics and developmental patterns of liver tumors, as different types of liver cancer display distinct diagnostic features during these phases. With advancements in deep learning, significant progress has been made in common computer vision tasks like image classification, object detection,

[1]West China Biomedical Big Data Center, West China Hospital; Med-X Center for Informatics, Sichuan University, Chengdu, 610044, China. [2]School of Communications and Information Engineering, Chongqing University of Posts and Telecommunications, Chongqing, 400065, China. [3]Department of Radiology, Chongqing Hospital of Traditional Chinese Medicine, Chongqing, 400000, China. [4]Department of Radiology, The People's Hospital of Yubei District of Chongqing city, Chongqing, 401120, China. [5]College of Biomedical Engineering, Chongqing Medical University, Chongqing, 400016, China. [6]Department of Scientific Research, The People's Hospital of Yubei District of Chongqing city, Chongqing, 401120, China. [7]School of Computer Science and Technology, Chongqing University of Posts and Telecommunications, Chongqing, 400065, China. ✉e-mail: d200101011@stu.cqupt.edu.cn; niexx@cqupt.edu.cn

and image segmentation[12,13]. Researchers have developed advanced models that have been widely applied and proven effective in the field of primary liver cancer[14–16]. Studies have shown that utilizing multi-phase CECT images of liver cancer enhances the identification of primary liver cancer subtypes, highlighting the importance of complete phase CECT data in building high-quality diagnostic models[17,18].

Currently, publicly available CECT datasets for primary liver cancer are limited, often focusing on a single type of cancer and lacking full phase imaging coverage. For example, the Liver Tumor Segmentation Benchmark (LiTS) dataset[19] only includes a few primary liver cancer subtypes such as HCC and ICC and does not provide comprehensive phase coverage. Similar issues exist in other datasets like the SLIVER07 dataset (https://sliver07.grand-challenge.org/), and some databases, such as the 3D-IRCADb and CHAOS datasets[20], have too few samples to support the training of classification or segmentation models. These data limitations hinder progress in accurately classifying liver cancer subtypes and precisely segmenting lesions. In response to these challenges, we have developed a 3D CECT dataset that includes various types of primary liver cancer with complete phase coverage. To help researchers distinguish between tumor and normal tissues, we also included CECT scans from patients without liver cancer as a control group. The purpose of constructing this dataset is to assist other research in better building deep learning models for classification or segmentation tasks using supervised learning. Although this dataset includes 278 primary liver cancer patients, which may seem limited for training models, it contains 50,560 annotated slices of lesions, carefully labeled by expert physicians. The dataset features three types of liver cancer: HCC, ICC, and cHCC-CCA, with each patient having complete 3D CECT images covering all four phases. This makes it a substantial and valuable resource for researchers. While the dataset primarily provides annotated liver and tumor lesion regions, it has potential clinical applications in the early detection, classification, and monitoring of primary liver cancer. For instance, it could aid in early diagnosis by identifying subtle changes in the liver's structure across different phases of CECT, which may help in detecting tumors at earlier stages. Additionally, the inclusion of multi-phase imaging data supports the development of models for liver cancer subtype classification (HCC, ICC, and cHCC-CCA), potentially leading to more accurate and personalized treatment plans. By utilizing this dataset, researchers can contribute to improving predictive models.

Despite the limitations of being a single-center dataset, which may necessitate additional data for model development and validation, we believe its public release will be valuable. It can be used as part of larger datasets from other sources or as an external validation set for other researchers.

Methods

We developed a 3D CECT dataset of primary liver cancer by retrospectively collecting and processing multi-phase scans. This involved data extraction, image conversion, segmentation, annotation by clinicians, de-identification, and validation to ensure data quality and consistency. Figure 1 gives an overview of the entire process.

Sample collection. All patients included in this study were sourced from the Radiology Department of Chongqing Yubei District People's Hospital between January 2015 and December 2022. To ensure data homogeneity and reliability, allowing for a focused investigation of primary liver cancer, we established specific inclusion and exclusion criteria.

The inclusion criteria were: (1) Patients primarily diagnosed with HCC, ICC, or cHCC-CCA. (2) Patients aged 18 years or older, regardless of gender. (3) Patients with liver masses whose resected or biopsy tissue specimens were confirmed as liver cancer through histological and/or cytological examination. The morphological codes were M81600/3 for ICC, M81700/3 for HCC, and M81800/3 for cHCC-CCA.

The exclusion criteria were: (1) Diagnosed non-primary liver cancers, such as liver cysts or hemangiomas. (2) Patients with confirmed primary liver cancer who had received any tumor-related treatment before inclusion in the study. (3) Patients with other primary malignant tumors of the digestive system or other systems, including leukemia and lymphoma. (4) Patients with conditions like hemochromatosis, Wilson's disease, autoimmune hepatitis, primary biliary cirrhosis, primary sclerosing cholangitis, Budd-Chiari syndrome, or schistosomal liver fibrosis/cirrhosis, as well as those with rheumatic or autoimmune diseases. (5) Patients with severe heart, brain, lung, or kidney diseases.

CECT acquisition and processing. In the retrospective data from the PACS system, each patient underwent a full multi-phase contrast-enhanced CT scan within two weeks before surgery. Abdominal imaging was performed using multi-detector CT scanners, specifically the Canon 64-slice Aquilion PRIME TSX-303A and the Philips 128-slice Brilliance iCT. For the Canon scanner, the arterial phase was triggered at a threshold of 180 HU with an 8-second delay, followed by a 60-second delay for the venous phase and a 180-second delay for the delayed phase. Similarly, for the Philips scanner, the arterial phase was triggered at 150 HU with an 8-second delay, followed by a 60-second delay for the venous phase and a 155-second delay for the delayed phase.

The imaging was performed with a Diameter Field of View (D-FOV) of 400.0 mm, a tube voltage of 120 kV. The matrix size was set to 512×512, with a contrast agent flow rate of 3 mL per second using Iohexol as the contrast medium. The scans were captured with a thin slice thickness of 0.8 mm and a rotation time of 0.5 milliseconds. A noise index of 14 was applied, with the automatic tube current modulation (AutoMA) ranging from 250 to 350 mA. All CECT image data were stored in DICOM format within the PACS system. It should be noted that images acquired from different devices were not calibrated for inter-device consistency.

Then, we extracted the CECT images from the PACS system, where they were initially stored as single-slice DICOM images. Using the SimpleITK package (https://pypi.org/project/SimpleITK/), we merged the single-slice DICOM images to create 3D CECT images, which were then saved in NIFTI format. Clinicians opened each phase of the 3D CECT images using the ITK-SNAP software and recorded the indices of all slices containing the liver region. Using these indices, we retained only the slices with liver regions and discarded the others. We then

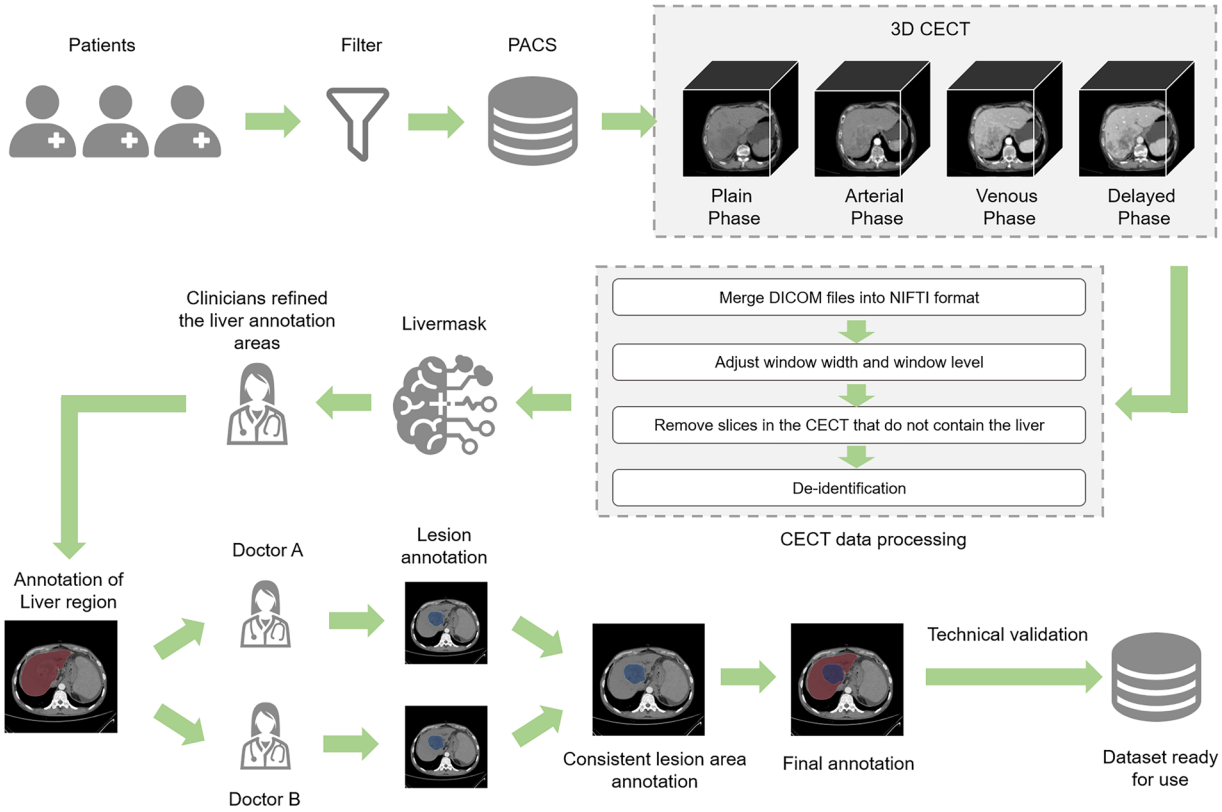

Fig. 1 An overview of the development process for our 3D CECT dataset of primary liver cancer. The process included sample selection, CECT data extraction, DICOM to NIFTI conversion, adjustment of window width and level, selection of slices containing the liver, de-identification, and liver annotation using a pre-trained model followed by clinician refinement. The lesion areas were independently annotated by two doctors, and any differences were reconciled. Finally, the dataset was validated for completeness and successful de-identification, resulting in the final labeled dataset.

adjusted the window width and window level of the liver CECT images by clipping the pixel intensity to a specified range (−200 to 200) using the NumPy package (https://pypi.org/project/numpy/). The window level was set to 0, and the window width to 400, which enhanced the clarity of liver anatomy and lesion areas in the images[21].

Next, we labeled the liver and lesion regions separately. For the liver region, we first used a pre-trained model from the LiverMask tool (https://github.com/andreped/livermask) to segment the liver in all images, saving the segmented regions in NIFTI format. Clinicians then refined the segmented liver masks using ITK-SNAP (Fig. 2). For the lesion region, the clinicians reviewed the non-contrast, arterial, venous, and delayed phase images simultaneously. During annotation, they considered the contrast-enhanced characteristics of the tumors at different phases. For example, tumors such as HCC often show high enhancement in the arterial phase, while some lesions may demonstrate washout in the venous phase. Clinicians were also mindful of the morphological features, such as irregular or lobulated tumor boundaries, and considered internal characteristics like necrosis, hemorrhage, or calcification, which may influence the lesion's appearance. However, it must be acknowledged that the annotation of tumor regions still involves a degree of subjectivity. Therefore, for each 3D CECT image, two independent clinicians performed separate annotations of the lesions. We then used the NumPy package to identify the slices with differences, and the two annotations were reviewed and modified by the clinicians together until they reached full agreement. The annotated data is shown in Fig. 3.

De-identification. When processing and preparing the image dataset for this study, we ensured compliance with privacy protection standards by de-identifying potential Protected Health Information (PHI) in the NIFTI file headers. Specifically, we cleared or updated fields such as database name, patient ID, description, and auxiliary file names to "Anonymized," removing any personally identifiable information. The modified files were then saved for subsequent research use. This straightforward and efficient method ensures that our data handling adheres to the requirements of the Health Insurance Portability and Accountability Act (HIPAA).

Technical Validation

To ensure the quality and usability of our 3D CECT dataset, we implemented several validation steps covering data integrity, consistency, and deidentification. These steps aimed to guarantee the reliability of our dataset for research and clinical applications.

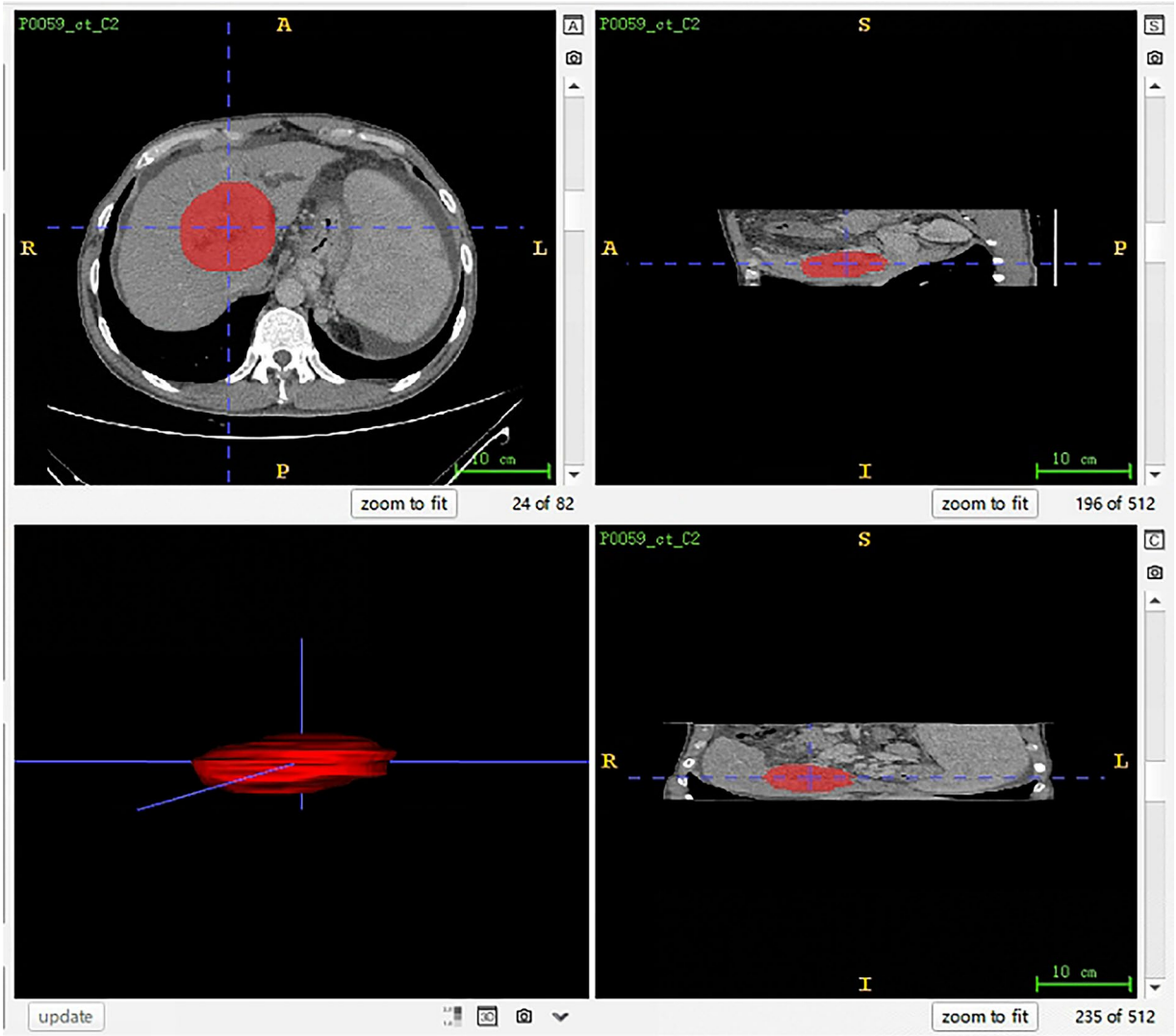

Fig. 2 3D visualization of liver tumor region annotations in axial, coronal, and sagittal planes. This figure displays a 3D visualization of a CECT image from a patient with ID "P0059" diagnosed with liver cancer. The top left panel shows the axial view of the liver with the annotated lesion region in red. The top right panel presents the coronal view, and the bottom left panel provides the sagittal view. The lesion region is consistently highlighted in red across all views, allowing for a comprehensive understanding of the tumor's location in 3D space. The bottom right panel presents the entire 3D structure, with the lesion marked in red, showing the extent of the tumor in relation to the surrounding liver tissue.

Our dataset underwent a series of automated and manual validation procedures to confirm its integrity and consistency across all phases. First, we verified that each CECT scan included all four phases (Non-Contrast, Arterial, Venous, and Delayed), and any missing or corrupted data files were flagged for review. During the image extraction process, we ensured that the conversion from DICOM to NIFTI format retained the full resolution and spatial properties of the original scans, preserving the accuracy of voxel dimensions and anatomical structures. We also implemented checks to verify that the number of slices annotated as containing liver regions matched the expected slice count based on the original DICOM images.

Our dataset included annotations created by two independent clinicians. To ensure the accuracy of these annotations, we performed an inter-observer validation by calculating the Dice coefficient for the overlap between the liver and lesion masks generated by each clinician. The mean Dice coefficient for inter-observer agreement was 0.7586, with a median of 0.7474, and a standard deviation of 0.0647. Discrepancies in annotations were reviewed, and final consensus masks were created. Additionally, to assess the volumetric agreement between radiologists, we calculated the tumor volume differences based on the annotated tumor regions. The mean volume difference was 55.78 cm^3, with a standard deviation of 107.47 cm^3. The median volume difference was 17.52 cm^3, indicating reasonable agreement with some variability, particularly for smaller tumors or those with larger discrepancies.

To comply with privacy regulations, we thoroughly de-identified the dataset. This included removing or anonymizing all potential identifiers in the NIFTI file headers after converting the images. We checked the

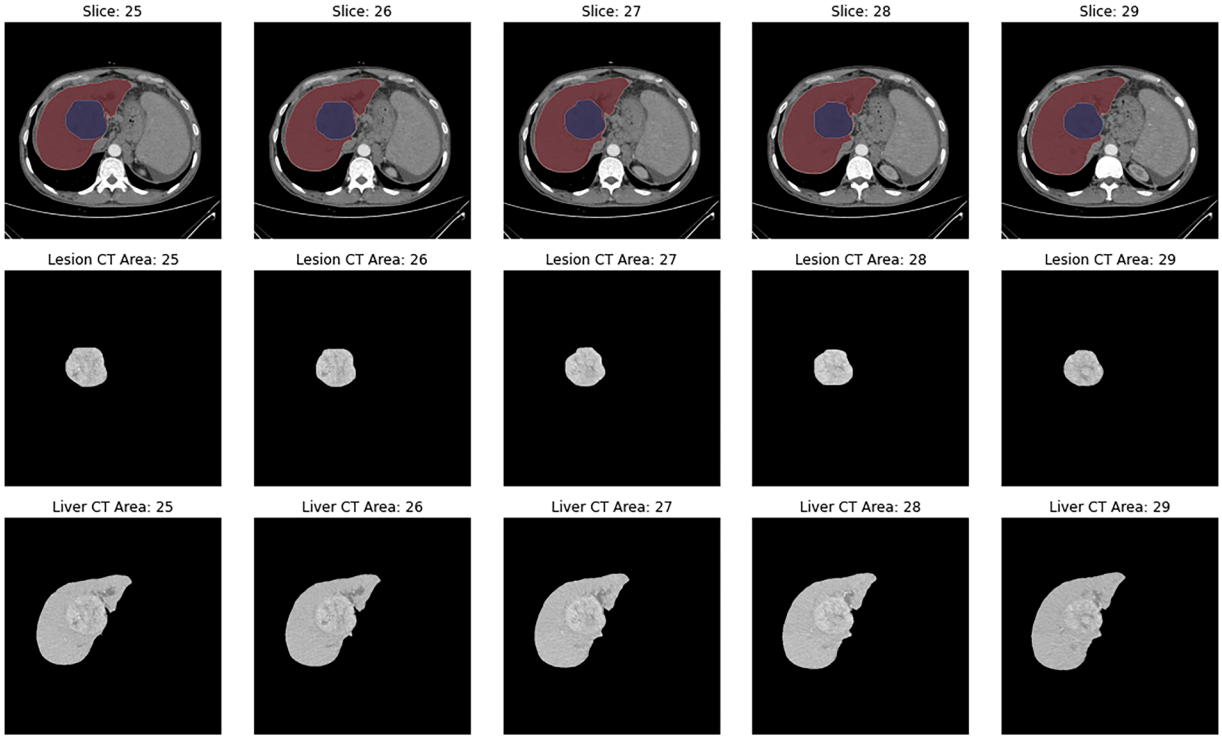

Fig. 3 Sample CECT image slice with segmentations. This figure presents CECT images from a patient with ID "P0059" diagnosed with HCC. The figure shows five consecutive slices from the arterial phase, all containing the lesion. The first row displays the annotated CECT images: red marks the liver region, and blue highlights the lesion. The second row shows the corresponding CT images of the lesion area, and the third row presents the CT images of the liver area.

success of this process by reviewing a random sample of NIFTI files to ensure that no protected health information remained.

Data Records

The data for this study are shared under a public access model on the Science Databank platform[22]. The dataset is published under a Creative Commons Attribution 4.0 International (CC BY 4.0) license, which permits unrestricted use, distribution, and reproduction in any medium, provided the original work is properly cited.

The dataset contains 3D contrast-enhanced CT (CECT) images for primary liver cancer patients and a control group. The CECT images are stored in NIFTI format and cover four imaging phases: Plain, Arterial, Venous, and Delayed. We stored each patient's 3D CECT data for each phase as separate NIFTI files. Alongside the images, NIFTI files for liver and lesion masks are provided. These masks were manually annotated by clinicians to highlight the liver and lesion regions. The lesion and liver region mask files were also saved as separate NIFTI files.

The dataset also includes a CSV file named "patient_data.csv," which serves as the metadata. This file contains patient-specific information, such as patient IDs, age, gender, cancer types, the imaging phases, and the file paths for both the CECT and mask data. Patients were re-identified with new IDs ranging from P0001 to P0361, and the corresponding CECT and mask file paths were saved in a CSV file, as shown in Fig. 4. All 3D CECT scans have dimensions of $n_{i,j} \times 512 \times 512$, where the number of slices $n_{i,j}$ may vary across different patients or different phases of the 3D CECT. The structure is organized to facilitate easy retrieval of corresponding files for each patient.

Data overview. Through sample selection, we identified 278 patients with primary liver cancer and 83 individuals without hepatobiliary disease as a control group. The diagnoses of liver cancer patients were confirmed by pathological examination. Table 1 shows the demographic characteristics, imaging phases, and lesion-related information for both groups. All individuals included in the study had complete 3D CECT imaging data across the Plain, Arterial, Venous, and Delayed phases.

For the liver cancer patients, there were 94 with HCC, 99 with ICC, and 85 with cHCC-CCA. The median age was 59 years [51, 67], and 67.3% (185) were male. These patients had 1,112 3D CECT images in total. A total of 50,560 slices with lesions were collected. Each liver cancer patient had a median of 124.00 slices [82.00, 188.00], including 37.00 slices with lesions [22.00, 59.25]. The median lesion volume was 75.37 cm^3 [26.70, 239.24]. The largest lesion volume was 5,987 cm^3, and the smallest lesion volume was 0.008 cm^3. The median maximum lesion diameter was 9.60 cm [6.66, 13.46], and the median lesion count per patient was 1.00 [1.00, 1.00].

For the non-liver cancer group, the median age was 41 years [37.50, 53.50], and 81.9% (68) were female. This group had 332 3D CECT images, covering the Plain, Arterial, Venous, and Delayed phases. All individuals in this group were confirmed to have no hepatobiliary disease, and no lesion data were collected.

patient_id	age	gender	phase	cancer_type	ct_path	mask_path	liver_mask_path
P0001	58	male	P	HCC	ct_files/P0001_ct_P.nii.gz	mask_files/P0001_mask_P.nii.gz	liver_mask_files/P0001-livermask_P.nii.gz
P0001	58	male	C3	HCC	ct_files/P0001_ct_C3.nii.gz	mask_files/P0001_mask_C3.nii.gz	liver_mask_files/P0001-livermask_C3.nii.gz
P0001	58	male	C2	HCC	ct_files/P0001_ct_C2.nii.gz	mask_files/P0001_mask_C2.nii.gz	liver_mask_files/P0001-livermask_C2.nii.gz
P0001	58	male	C1	HCC	ct_files/P0001_ct_C1.nii.gz	mask_files/P0001_mask_C1.nii.gz	liver_mask_files/P0001-livermask_C1.nii.gz
P0002	70	male	C2	HCC	ct_files/P0002_ct_C2.nii.gz	mask_files/P0002_mask_C2.nii.gz	liver_mask_files/P0002-livermask_C2.nii.gz
P0002	70	male	C3	HCC	ct_files/P0002_ct_C3.nii.gz	mask_files/P0002_mask_C3.nii.gz	liver_mask_files/P0002-livermask_C3.nii.gz
P0002	70	male	P	HCC	ct_files/P0002_ct_P.nii.gz	mask_files/P0002_mask_P.nii.gz	liver_mask_files/P0002-livermask_P.nii.gz
P0002	70	male	C1	HCC	ct_files/P0002_ct_C1.nii.gz	mask_files/P0002_mask_C1.nii.gz	liver_mask_files/P0002-livermask_C1.nii.gz
P0003	66	female	P	HCC	ct_files/P0003_ct_P.nii.gz	mask_files/P0003_mask_P.nii.gz	liver_mask_files/P0003-livermask_P.nii.gz
P0003	66	female	C3	HCC	ct_files/P0003_ct_C3.nii.gz	mask_files/P0003_mask_C3.nii.gz	liver_mask_files/P0003-livermask_C3.nii.gz
P0003	66	female	C2	HCC	ct_files/P0003_ct_C2.nii.gz	mask_files/P0003_mask_C2.nii.gz	liver_mask_files/P0003-livermask_C2.nii.gz
P0003	66	female	C1	HCC	ct_files/P0003_ct_C1.nii.gz	mask_files/P0003_mask_C1.nii.gz	liver_mask_files/P0003-livermask_C1.nii.gz
⋮							

Fig. 4 Sample table showing patient IDs and corresponding 3D CECT and mask file paths. cHCC-CCA: Combined Hepatocellular-Cholangiocarcinoma; HCC: Hepatocellular Carcinoma; ICC: Intrahepatic Cholangiocarcinoma.

Category	Liver Cancer Patients (N = 278)	Non-Liver Cancer Patients (N = 83)
Number of patients (N)	278	83
Age (years) (median [IQR])	59.00 [51.00, 67.00]	41.00 [37.50, 53.50]
Gender (%)		
Male	185 (67.3)	15 (18.1)
Female	90 (32.7)	68 (81.9)
Total number of 3D CECT images (N)	1112	332
Phases (%)		
Arterial Phase	278 (25.0)	83 (25.0)
Venous Phase	278 (25.0)	83 (25.0)
Delayed Phase	278 (25.0)	83 (25.0)
Plain Phase	278 (25.0)	83 (25.0)
Cancer type (%)		
cHCC-CCA	85 (30.6)	—
HCC	94 (33.8)	—
ICC	99 (35.6)	—
Normal	—	83 (100.0)
Total number of CT slices (N)	152965	53295
Total number of CT slices with lesions (N)	50560	—
Slices per patient (median [IQR])	124.00 [82.00, 188.00]	175.50 [48.75, 200.25]
Slices with lesions per patient (median [IQR])	37.00 [22.00, 59.25]	—
Lesion volume (cm^3) (median [IQR])	75.37 [26.70, 239.24]	—
Max lesion diameter (cm) (median [IQR])	9.60 [6.66, 13.46]	—
Lesion count (median [IQR], (minimum, maximum))	1.00 [1.00, 1.00], (1, 27)	—

Table 1. Summary of Basic Data Information. cHCC-CCA: Combined Hepatocellular-Cholangiocarcinoma; HCC: Hepatocellular Carcinoma; ICC: Intrahepatic Cholangiocarcinoma.

Usage Notes

The dataset supporting this study has been deposited in the Science Data Bank and is publicly available at https://doi.org/10.57760/sciencedb.12207, under the Creative Commons Attribution 4.0 International (CC BY 4.0) license[22]. Users are free to download, use, and redistribute the dataset, including for commercial purposes, provided proper attribution is given to the original authors.

For data analysis, we have provided Python code in a GitHub repository (https://github.com/ljwa2323/PLC_CECT). The repository includes a file named demo.ipynb, which demonstrates how to load the dataset using the file paths specified in the patient_data.csv file.

Ethics Approval and Consent to Participate

This study received approval from the Ethics Committee of Chongqing Yubei District People's Hospital (Approval No. 2022SA11) to conduct the study and share the data. Due to the retrospective design of the study, the committee waived the requirement for informed consent.

Code availability

The code we used to merge DICOM files into NIFTI format, remove non-liver CECT slices, and adjust window width and level, along with example code for loading patient data, can be found at https://github.com/ljwa2323/PLC_CECT.

Received: 28 August 2024; Accepted: 1 May 2025;
Published online: 10 May 2025

References

1. Rumgay, H. *et al*. Global burden of primary liver cancer in 2020 and predictions to 2040 [J]. *Journal of Hepatology* **77**(6), 1598–606 (2022).
2. Qin, Y. *et al*. Liver cancer in China: the analysis of mortality and burden of disease trends from 2008 to 2021 [J]. *BMC cancer* **24**(1), 594 (2024).
3. Yildirim, H. Ç. *et al*. Advances in the early detection of hepatobiliary cancers [J]. *Cancers* **15**(15), 3880 (2023).
4. Garancini, M. *et al*. Combined hepatocellular-cholangiocarcinoma: a population-level analysis of an uncommon primary liver tumor [J]. *Liver Transplantation* **20**(8), 952–9 (2014).
5. Yang, J. D. & Roberts, L. R. Management of combined hepatocellular carcinoma-cholangiocarcinoma [J]. *Current hepatology reports* **17**, 385–91 (2018).
6. Sung, H. *et al*. Global cancer statistics 2020: GLOBOCAN estimates of incidence and mortality worldwide for 36 cancers in 185 countries [J]. *CA: a cancer journal for clinicians* **71**(3), 209–49 (2021).
7. Zhou, J. *et al*. Guidelines for the diagnosis and treatment of hepatocellular carcinoma (2019 edition) [J]. *Liver cancer* **9**(6), 682–720 (2020).
8. Kinoshita, M. *et al*. Deep learning model based on contrast-enhanced computed tomography imaging to predict postoperative early recurrence after the curative resection of a solitary hepatocellular carcinoma [J]. *Cancers* **15**(7), 2140 (2023).
9. Yang, J. *et al*. Comparison contrast-enhanced CT with contrast-enhanced US in diagnosing combined hepatocellular-cholangiocarcinoma: a propensity score-matched study [J]. *Insights into Imaging* **15**(1), 44 (2024).
10. Li, R. *et al*. Combined hepatocellular carcinoma and cholangiocarcinoma (biphenotypic) tumors: clinical characteristics, imaging features of contrast-enhanced ultrasound and computed tomography [J]. *BMC cancer* **16**, 1–11 (2016).
11. Willatt, J. *et al*. Imaging of hepatocellular carcinoma and image guided therapies-how we do it [J]. *Cancer Imaging* **17**, 1–10 (2017).
12. Pouyanfar, S. *et al*. A survey on deep learning: Algorithms, techniques, and applications [J]. *ACM computing surveys (CSUR)* **51**(5), 1–36 (2018).
13. Talaei Khoei, T., Ould Slimane, H. & Kaabouch, N. Deep learning: Systematic review, models, challenges, and research directions [J]. *Neural Computing and Applications* **35**(31), 23103–24 (2023).
14. Lee, I.-C. *et al*. A hierarchical fusion strategy of deep learning networks for detection and segmentation of hepatocellular carcinoma from computed tomography images [J]. *Cancer Imaging* **24**(1), 43 (2024).
15. Hettihewa, K. *et al*. MANet: a multi-attention network for automatic liver tumor segmentation in computed tomography (CT) imaging [J]. *Scientific Reports* **13**(1), 20098 (2023).
16. Wu, Y. *et al*. Automatic liver tumor segmentation used the cascade multi-scale attention architecture method based on 3D U-Net [J]. *International Journal of Computer Assisted Radiology and Surgery* **17**(10), 1915–22 (2022).
17. Gao, R. *et al*. Deep learning for differential diagnosis of malignant hepatic tumors based on multi-phase contrast-enhanced CT and clinical data [J]. *Journal of hematology & oncology* **14**(1), 1–7 (2021).
18. Khan, R. A. *et al*. A multi-modal deep neural network for multi-class liver cancer diagnosis [J]. *Neural Networks* **165**, 553–61 (2023).
19. Bilic, P. *et al*. The liver tumor segmentation benchmark (lits). *JJ. Medical Image Analysis* **84**, 102680 (2023).
20. Singh, S. *et al*. Radiological diagnosis of chronic liver disease and hepatocellular carcinoma: A review [J]. *Journal of Medical Systems* **47**(1), 73 (2023).
21. Xu, W. *et al*. Liver segmentation in CT based on ResUNet with 3D probabilistic and geometric post process; proceedings of the 2019 *IEEE 4th International Conference on Signal and Image Processing (ICSIP)*, F, 2019 [C]. IEEE.
22. Luo,J. *et al*. Primary Liver Cancer CECT Imaging Dataset [Data set]. *Science Data Bank*. Version 3. https://doi.org/10.57760/sciencedb.12207 (2025).

Acknowledgements

This research was supported by Chongqing medical scientific research project, a joint project of Chongqing Health Commission and Science and Technology Bureau (Grant Numbers: 2025QNXM034); the Sichuan Science and Technology Program (Grant Number: 2023YFS0200); and the Foundation Sciences of The People's Hospital of Yubei District of Chongqing City (Grant Numbers: ybyk2023-04, 2023). The authors thank all contributors involved in data acquisition and preprocessing.

Author contributions

Doctors Jinchao Du and Min Wu were responsible for data annotation, while Jiawei Luo and Xixi Nie handled programming and data visualization. Xiaoyu Wan and Xin Peng supervised the project, and Li Liu and Ling Zhao were in charge of data verification. Shixin Huang managed data extraction and overall data management. All authors contributed to initiating the project, and everyone participated in writing and reviewing the manuscript.

Competing interests

The authors declare no competing financial or non-financial interests.

Additional information

Correspondence and requests for materials should be addressed to S.H. or X.N.